On the Influence of Estuarine Outflow and Bathymetry on Semidiurnal Tidal Currents

Andrew G.E. Haskell[*]
Arnoldo Valle-Levinson[*]
Kamazima M.M. Lwiza[†]

[*] Center for Coastal Physical Oceanography
Old Dominion University
Norfolk, VA 23529

[†] Marine Sciences Research Center
State University of New York
Stony Brook, NY 11794-5000

Submitted to Continental Shelf Research

ABSTRACT

Current velocity profiles from an Acoustic Doppler Current Profiler (ADCP) were used to investigate the influence of estuarine outflows and bathymetry on the semidiurnal tidal flow along a cross-shore transect outside of the Chesapeake Bay. The shelf transect was repeated eight times during one neap tidal cycle on March 26-27, 1996 under the effects of a well-defined Chesapeake Bay plume. The bathymetry of the transect featured an 18 m deep channel flanked by 10 m shoals to the sides. The observations showed that the maximum subtidal velocity perpendicular to the transect was associated with the plume outflow, reaching values of nearly 0.6 m s^{-1}. The mean flow parallel to the transect had typical values of 0.1 m s^{-1}, which could have been related to a quasi-geostrophic flow within the turning region of the plume. The amplitude and phase of the tidal flow inside the bay plume were significantly different from those of the underlying shelf water. The plume outflow caused the surface tidal flow to lag behind the near-bottom frictionally influenced flow by 40 degrees (~80 minutes). The tidal amplitude exhibited a subsurface maximum that was centered over the channel. The channel location of the maximum amplitude reflected frictional influences and the subsurface location was explained with the output of a one-dimensional mixed-layer model. The mixed-layer model showed that the subsurface maximum in tidal amplitude developed under the combined influence of various factors: large horizontal salinity gradients (4 units in 10 km), relatively weak tidal (0.5 m s^{-1}) and wind forcing (< 0.1 Pa), and over relatively deep (> 15 m) regions as was observed in the field. The subsurface maximum appeared at the base of the pycnocline where turbulence was suppressed, which was indicated by zero vertical eddy viscosities. Any modification to those factors caused the maximum to appear at the surface.

INTRODUCTION

The outflow of low-salinity estuarine water into the ocean forms a plume that tends to deflect anticyclonically in the Northern Hemisphere and form a boundary current with the coastline on its right-hand side (*e.g.* Münchow *et al.*, 1992). The current scope of information on the interaction between these estuarine outflows and the tidal currents on the shelf is restricted to idealized numerical experiments performed over narrow (width smaller than one internal radius of deformation) inlets (Kapolnai *et al.*, 1996; Wheless and Valle-Levinson, 1996). This interaction, jointly with wind influences, ultimately determines the fate of suspended and dissolved matter and biota that can be found near the estuary mouth.

Estuarine plumes derived from wide systems have been studied by numerical methods that ignore tidal influences or that use distantly spaced data, for example, moored instruments or density profiles (*e.g.* Münchow *et al.*, 1992; Weaver and Hsieh, 1987; Chao, 1988; Chao and Boicourt, 1986). More recently, with the Acoustic Doppler Current Profiler (ADCP), current data can be measured on relatively fine spatial scales. A horizontal resolution of approximately 60-75 m is attained with 30 second ensembles (or averages) and cruising speeds of 4-5 knots. This resolution is sufficient to study general features of estuarine plumes like those from the Chesapeake Bay, which is a typical example of wide (width greater than one internal radius of deformation) estuarine plumes.

The Chesapeake Bay is located in the mid-Atlantic region of the United States and is the largest estuary in the country. The temporal variability of the flow through the mouth of the Chesapeake Bay is dominated by tidal forcing (*e.g.* Browne and Fisher, 1988), but wind forcing and freshwater discharge also may produce important variations (*e.g.* Valle-Levinson, 1995; Valle-Levinson and Lwiza, 1997). The spatial variability of the flow in the lower Chesapeake Bay is greatly influenced by the bathymetry (Valle-Levinson and Lwiza, 1995).

The bathymetry of the inner continental shelf, near the entrance to the Chesapeake Bay, is characterized by a channel (Fig. 1) that is expected to cause spatial variability in the flow. It is also expected to influence the formation of frontal features along the region of the channel with the greatest bathymetry curvature, as in the Delaware Bay coastal current (Sanders and Garvine, 1996). Currently, little is known about how the Chesapeake Bay plume structure varies with the tidal cycle because it is difficult to avoid tidal aliasing inherent to surveys of high spatial resolution and several kilometers extent. Also, little is known about the influences of plume outflow and of the bathymetry on the tidal flows. Several studies have shown that a rapid change in water depth is a controlling factor in determining the position of tidally induced fronts (*e.g.* Largier, 1992; Huzzey, 1982; and Largier and Taljaard, 1991). These fronts may form at the mouths of estuaries when inner shelf flood waters meet buoyant estuarine waters.

The purpose of this study was to describe the effects that a plume of buoyant water flowing from an estuary to an inner shelf with abrupt bathymetry had on the tidal currents. These effects were assessed in terms of the spatial distribution of tidal amplitude and phase along a section influenced by the Chesapeake Bay outflow. The present study differed from previous ones in that it was the first to report on a complete cross-section of a freshwater plume using the high resolution capabilities of the ADCP. Other studies have used ADCPs to measure different

characteristics of the tidal currents (*e.g.*, Simpson and Souza, 1995; Souza and Simpson, 1996; Sanders and Garvine, 1996) however none of these examined the features addressed in this study.

Both Souza and Simpson (1996) and Simpson and Souza (1995) used a combination of seabed mounted ADCPs and moored current meters to gather current data at distinct points. Sanders and Garvine (1996) did perform a repeated transect using an ADCP but only reported results at several locations instead of a continuous cross section as presented here. In addition to advancing the general knowledge of the effects of buoyancy outflow and bathymetry on tidal currents, this study described the influence of the vertical eddy viscosity, as influenced by tidal currents and wind forcing, on the vertical profile of the tidal current amplitude.

STUDY AREA

The study area was located to the south of the Chesapeake Bay mouth, approximately 8 km south of Cape Henry (Fig. 1). The bathymetry is characterized by a complex system of shoals and navigational channels. The mean depth of the region is approximately 10 m with depths reaching 30 m over Chesapeake Channel off Cape Henry. This channel follows the coastal morphology at the inner shelf and shoals rapidly to the south. The influence of this bathymetry on tidal amplitude and phase outside of the bay mouth is essentially unknown. Also, little is known about the direction and magnitude of the tidal currents off the Virginia Beach coast. It is recognized that the principal constituent of the tidal energy of the area is the lunar semidiurnal

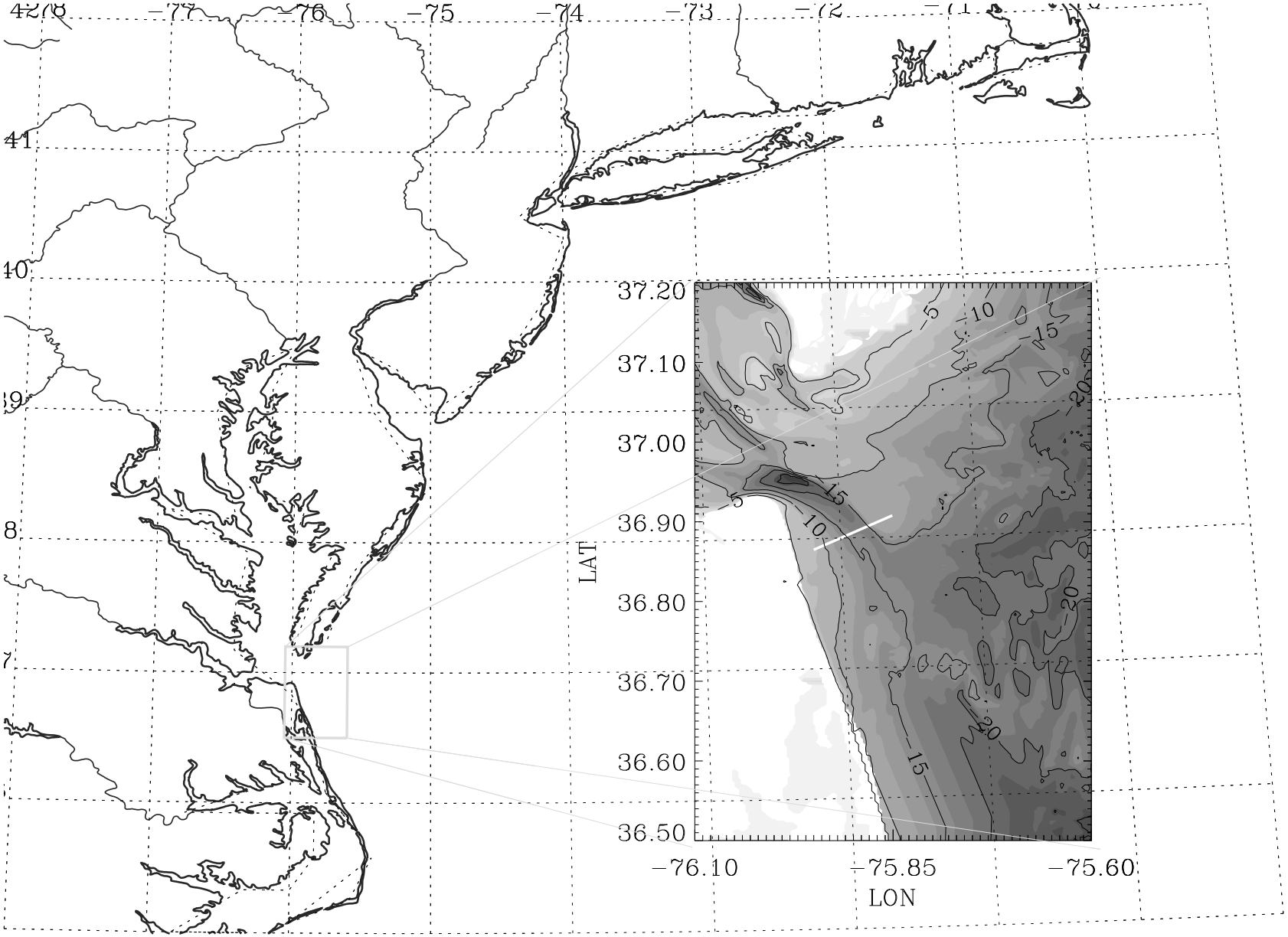

Figure 1. Lower Chesapeake Bay and inner continental shelf. Inset shows the location of the transect studied (white line) and the bathymetry of the area including the Chesapeake Channel. The bathymetry is contoured at 10m intervals. The transect ran nearly perpendicular to the coastline and started 3 km off the Virginia Beach coast and extended approximately 10 km seaward.

(M_2) (Fisher, 1986; Browne and Fisher, 1988) and that the tidal phase in the Mid-Atlantic Bight propagates northward from Cape Hatteras (Redfield, 1958). Further details are explored in this work.

The influence of the plume generated by the Chesapeake Bay outflow on the shelf produces, in general, southward subtidal surface currents off Virginia Beach (Boicourt, 1973; 1981). The shape and extension of the plume and its outflow are affected by wind forcing. Northeasterly winds cause the plume to accelerate, lengthen and narrow while winds from the southwest decelerate and widen the plume (Boicourt, 1981). The near-bottom subtidal flow is likely to be affected by wind direction but a clear pattern of response has not yet been identified. This near-bottom flow may move in the same direction of the wind or in opposite direction depending on water column stratification (Johnson, 1985). Wind forcing in the vicinity of the Chesapeake Bay entrance typically tends to be strongest and northeasterly in the fall and winter, and weakest and southwesterly in the summer (Paraso and Valle-Levinson, 1996).

DATA ACQUISITION

Current velocity profiles and near-surface temperature and salinity were obtained along one transect that started 3 km off the Virginia Beach coast and extended approximately 10 km seaward. Current velocity measurements consisted of towing a broadband 600 kHz RD Instruments ADCP. The ADCP was towed looking downward from the NOAA ship *R/V Ferrel* at a speed of approximately 2 m s^{-1} (4 kn). Navigation was carried out with a differential Global Positioning System (DGPS). The length of the transect was chosen to accommodate the greatest extension possibly covered in 1.5 hrs while sampling continuously at 2 m s^{-1}. The transect ran perpendicular to the coastline that parallels the Chesapeake Channel (Fig. 1). The objective of the sampling scheme was to complete as many repetitions as possible within one tidal cycle to effectively distinguish the tidal signal from the records. Eight repetitions of the transect were completed on 26-27 March 1996 within 12.5 hours. Sampling occurred with NNE winds of 5-7 m s^{-1}, following a 36 hour period of SSE winds of ~5 m s^{-1}. Sampling also coincided with a period of large freshwater discharge. For one month prior to the survey, freshwater discharge was more than 3 times (~7600 m^3 s^{-1}) the 46-year average for the Chesapeake Bay (~2200 m^3 s^{-1}) (United States Geological Survey -USGS- press releases on the World Wide Web).

Each ADCP profile represented a 30 second average of approximately 120 pings. The ADCP velocities were separated vertically into 0.5 m bins with an approximate horizontal spacing of 200 m. Data with error velocities (the difference between the redundant vertical velocities) greater than 0.08 m s^{-1} were discarded. The bin closest to the surface was centered at a depth of 2.75 meters. The sampling period at each gridded location varied from ~80 minutes over the mid-channel to a range of 10 to 160 min over the shoals near the ends of the transect. Data from the ends of each repetition were discarded to ensure a ten-minute minimum interval between the locations defined as the ends of the transect. Also, data collected while moving to avoid traffic were discarded. The ADCP velocities were calibrated as in Joyce (1989), which yielded a misalignment angle of -1.023° and a scaling factor of 1.0603. The data were then rotated from the earth's coordinate frame to a frame representing along and across channel (along and across shore) directions (12° west of north). Finally the data were interpolated to a uniform grid of 48 points in the horizontal and 33 in the vertical.

The time series of eight values at each grid-point was fitted, using least squares, to a sinusoid with an M_2 period (12.42 hours) as in Lwiza *et al.* (1991). This procedure produced the subtidal flow (periods greater than semidiurnal) along with the semidiurnal tidal amplitude and phase at each grid point. Along-channel and across-channel components were treated separately. The fifth repetition of the transect showed noisy values and was discarded from the least squares analysis. This elimination reduced the overall root mean square error values by 0.07 m s^{-1} in the along-shore direction and by 0.20 m s^{-1} in the across-shore direction.

Simultaneously to current profiling, near-surface temperature and salinity were measured by continuously pumping water from a depth of ~1 m through a Sea Bird 1621 thermosalinograph with a sampling interval of 10 s. The near surface temperature and salinity were also fitted to a semidiurnal sinusoid to obtain the subtidal structure along the transect. Vertical profiles of salinity and temperature were not collected in order to optimize the ADCP data quality and their time of acquisition.

DESCRIPTION OF OBSERVATIONS

First, the structure of the estuarine outflow was described in terms of the subtidal flow and salinity fields. The bathymetric influence on the estuarine outflow was also explored through examination of subtidal fields. Second, the effects of bathymetry and of estuarine outflow on the semidiurnal tidal currents were described in terms of the tidal fields. The interpretation of the effects of estuarine outflow on tidal currents was supported by the output of a mixed layer model.

Subtidal Fields

The along-channel subtidal flow (Fig. 2) showed southward flow throughout the section studied. Maximum values reached 0.55 m s^{-1} in the region that was most likely related to the core of the Chesapeake Bay outflow. These magnitudes seemed consistent with a surface to bottom density difference of O(10 kg m^3) (Turner, 1973), which agreed with the strongest stratification observed in the lower Chesapeake Bay during spring tides in March 1996 (unpublished data). This large subtidal flow could have been a result of the barotropic forcing, from high river discharge and southwestward winds, combined with the baroclinic forcing, from the large density gradients. However, there was no evidence of the influence of baroclinic forcing as the subtidal along-shore current flowed only in one direction. As shown by Noble *et al.* (1996) large river discharges drove near-bottom currents in the direction of the discharge. This suggested that the subtidal flow observed, which consisted of a relatively sluggish southward ambient flow (0.10 - 0.15 m s^{-1}) underlying a relatively swift surface plume, was primarily driven by river discharge and wind forcing. The integrated transport through the observed section was 14,485 m^3 s^{-1}. The monthly averaged freshwater discharge into the bay during February and March of 1996 was approximately 4000 m^3 s^{-1} which corresponded to the area of the plume extending approximately 5.5 m deep and 5.5 km from the start of the transect. The remaining 10,000 m^3 s^{-1} could possibly be supplied by the ambient coastal current flowing southward at the observed rate of 10 cm s^{-1}.

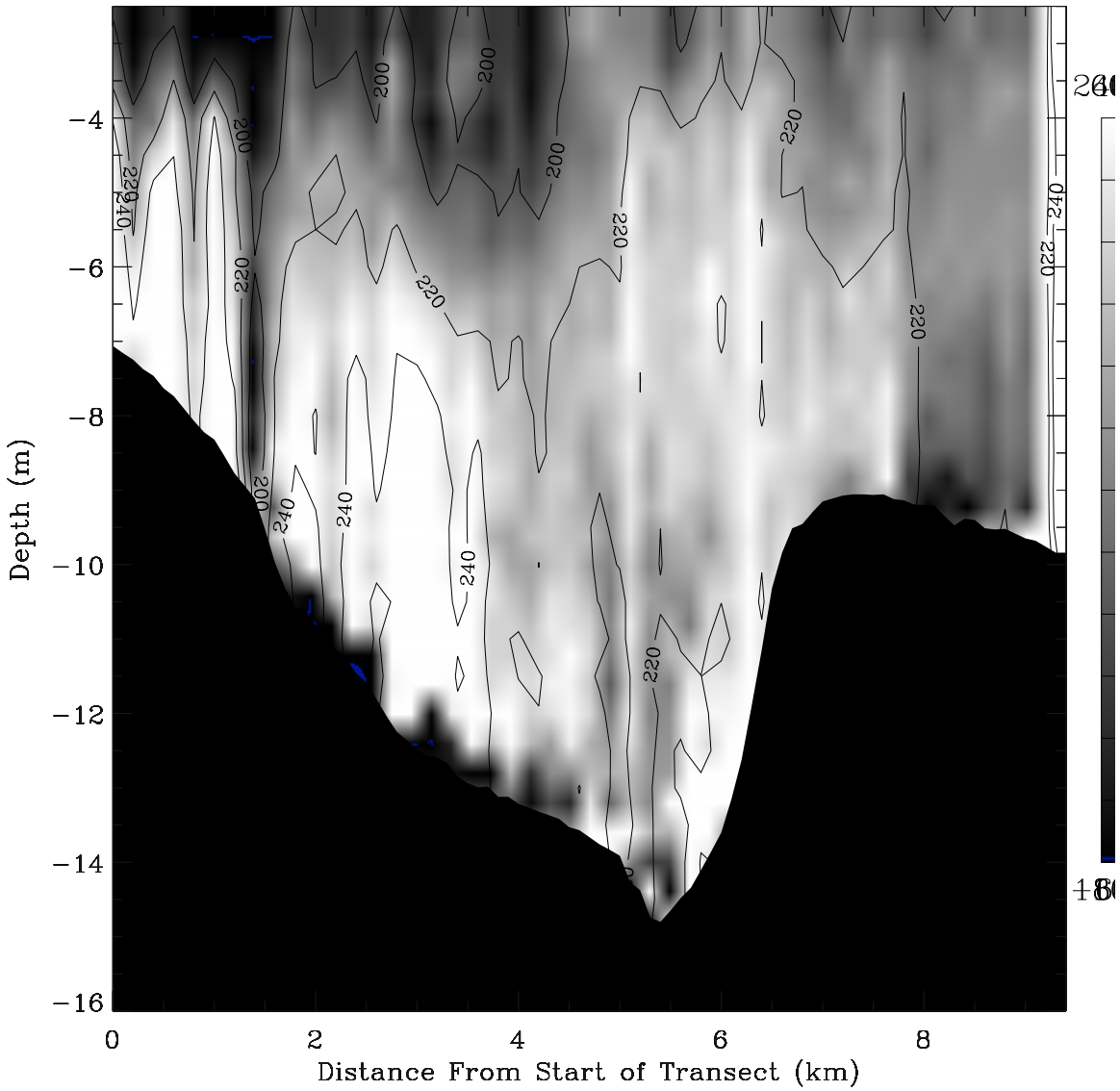

Figure 2. Lower Chesapeake Bay and inner continental shelf. Inset shows the location of the transect studied (white line) and the bathymetry of the area including the Chesapeake Channel. The bathymetry is contoured at 10m intervals. The transect ran nearly perpendicular to the coastline and started 3 km off the Virginia Beach coast and extended approximately 10 km seaward

The across-channel subtidal flow was comparatively weaker than the along-channel flow (Fig. 3). It was negative (shoreward) practically everywhere along the section and the highest values appeared near the surface. The negative character of both subtidal flow components indicated a southwestward flow that probably resulted from the Coriolis accelerations acting on the flow produced by river and wind forcing. It is likely that the sampling transect was located within the quasi-geostrophic anticyclonic or turning region of the outflow plume, as suggested by the numerical results of Chao (1988) and Valle-Levinson *et al.* (1996).

The surface salinity and temperature values (Fig. 4) showed the plume offshore front existing at the same location over the channel as suggested by the along-shore subtidal flow. Although only one distinct along channel front was evident in the present study, a near shore front was also noted visually during the cruise but was shoreward of our sampling limit. The existence of two fronts over the maximum concave curvature of a channel connecting to an estuary mouth was also noted by Sanders and Garvine (1996) for the Delaware Bay coastal current. The bathymetry and the inertia of the plume leaving the bay mouth caused the bulk of the plume to separate from the coast, producing both offshore and onshore fronts, before Coriolis acceleration organized the flow in a southward coastal current as suggested by the numerical models of Chao and Boicourt(1986), Chao(1988), and Valle-Levinson *et al.* (1996). The amplitude of the surface salinity variation was related to the amplitude of the along-channel semidiurnal flow (as presented later). This was a reflection of the elastic straining of the salinity field by the tidal currents.

Tidal Fields

The first effect of the estuarine outflow on the tidal fields was noticed in the phase of the M_2 along-shore tidal current. The phase showed near surface lags of 80 min (40 degrees) in an area that was presumably associated with the southward flowing Chesapeake Bay plume (Fig. 5). This indicated that the tidal currents near the surface lagged behind the underlying shelf water. The phase lag within the plume was consistent with the upward propagation of the tidal phase and with the decoupled dynamics between the baroclinically driven buoyant outflow and the barotropically driven interior flow. The phase lag was due to the combined effects of friction and inertia that allowed a faster response of near-bottom flows to tidal forcing (Valle-Levinson and Lwiza, 1995). The greatest phase lag was laterally delimited by sharp bathymetric changes, which also suggested a bathymetric delimitation of the outflow plume as in the Delaware Bay (Sanders and Garvine, 1996). In general, the water inside the channel responded more slowly to tidal forcing than the surrounding water, which was probably related to the distinct hydrographic characteristics in the channel as observed in the lower Chesapeake Bay (Valle-Levinson and Lwiza, 1997), where the channel flow tends to favor the flood direction due to baroclinic inflow.

Additional effects of bathymetry and buoyant outflow on the tidal currents were evident in the distribution of the amplitude of the along-shore component. The maximum amplitude of the along-channel M_2 flow was found over the channel at approximately 6 km from the coast (Fig. 6) similarly to Münchow *et al.* (1992) and Valle-Levinson and Lwiza (1995). This was a consequence of reduced frictional effects over the deeper areas. An interesting finding was that the maximum appeared at a depth of 5.5 m and not near the surface, where the largest amplitude is usually expected because of the greatest distance from bottom frictional effects. The subsurface location of the strongest semidiurnal tidal currents could have coincided with the pycnocline that delimited the plume outflow, which effectively decreased frictional effects through a reduction of

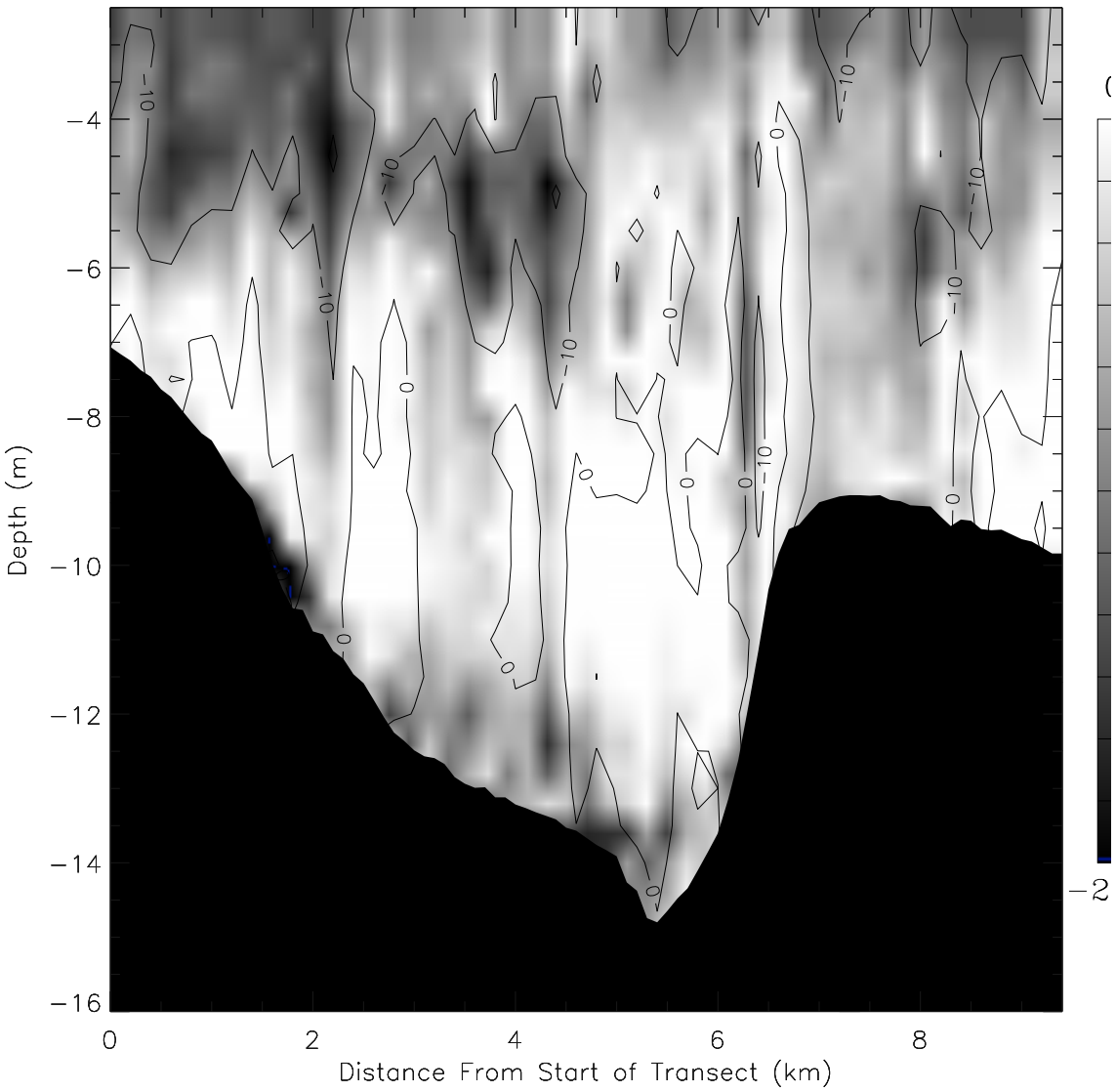

Figure 3. Across-channel subtidal flow (centimeters per second) along the cross section studied. Contour interval is 10 cm s^{-1}, negative values represent westward or shoreward flows. Dark regions represent high values.

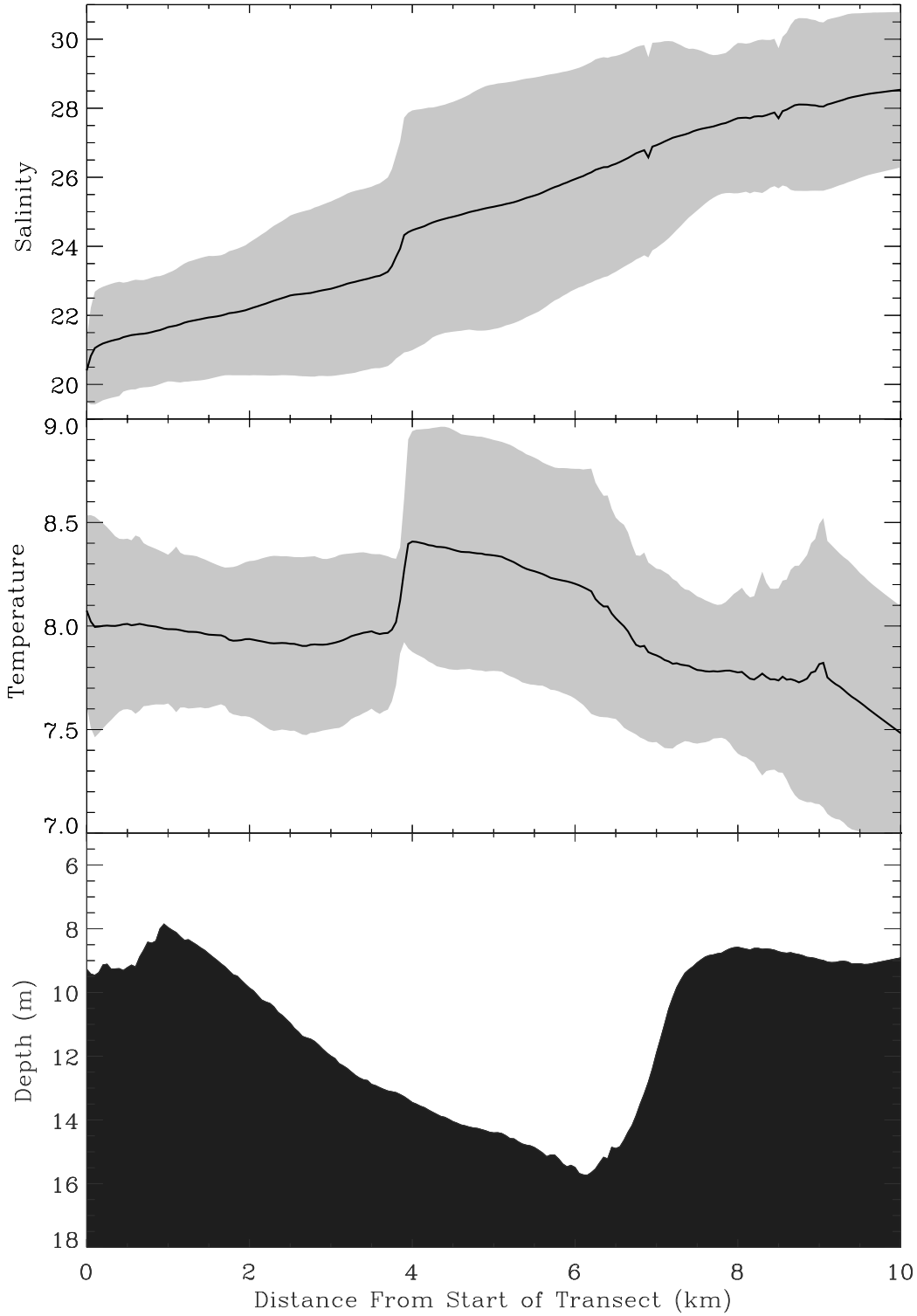

Figure 4. Surface salinity (top) and temperature (middle, °C) values shown over the bathymetry (bottom) of the transect studied. The dark line in the top two panels denotes the mean value of all 8 repetitions while the shaded area shows the rmse range.

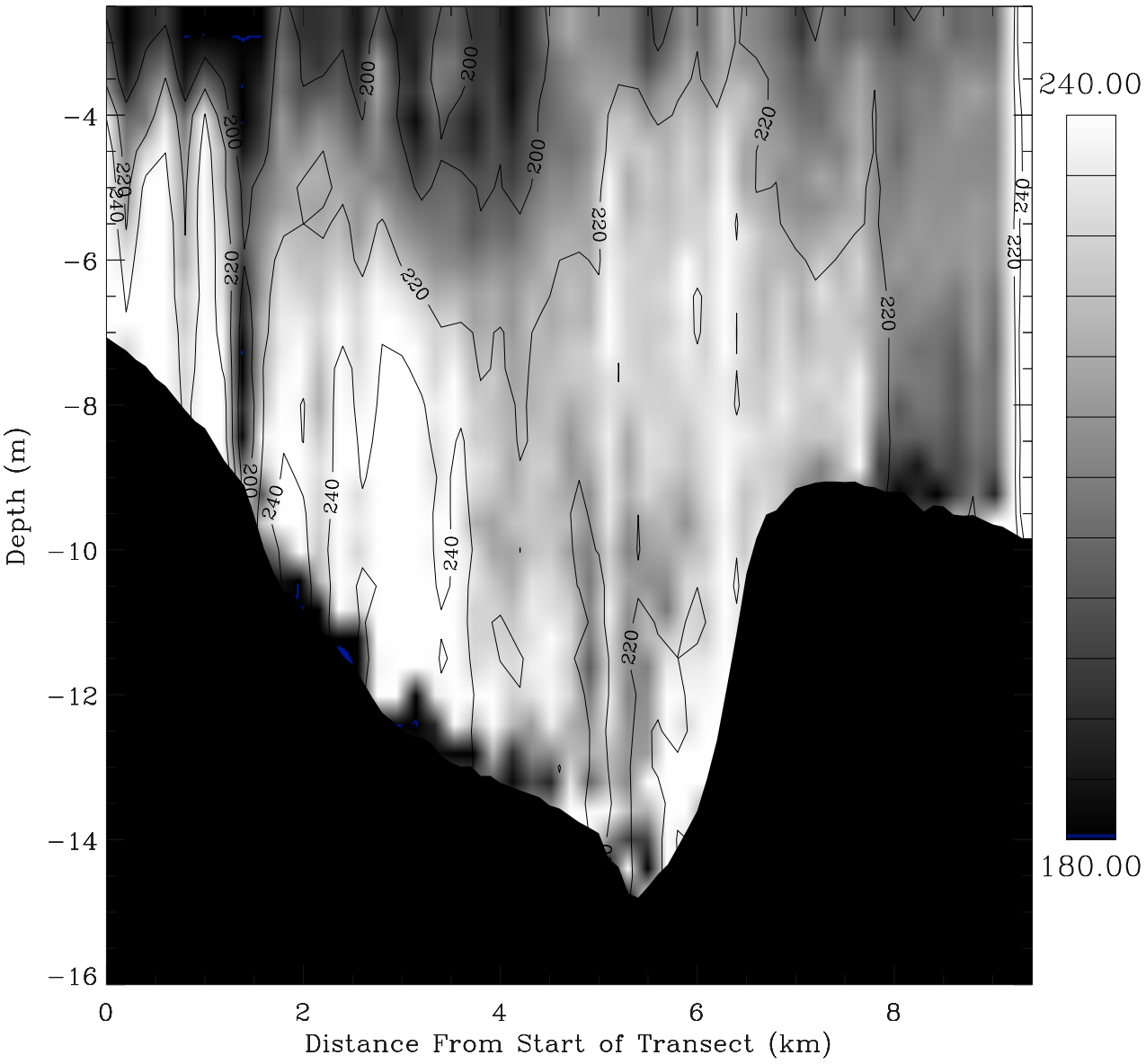
240.00
180.00
Depth (m)
−4
−6
−8
−10
−12
−14
−16
0
2
4
6
8
Distance From Start of Transect (km)

the eddy viscosity and of turbulence. The influence of the density field (plume outflow) on the eddy viscosity and in turn on the tidal current amplitude was addressed with a simplified one-dimensional mixed layer model presented next.

MIXED LAYER MODEL

A total of eight process-oriented experiments with a mixed layer model helped to elucidate the effects of buoyant outflow on the tidal current amplitude as observed outside the Chesapeake Bay mouth. The eight experiments performed are summarized in Table 1. Experiment 1 looked at the effect of the plume on weak tidal currents and constituted the base case. Experiment 2 investigated the same influence under strong tidal currents. Experiment 3 extended the effects of Experiment 1 to include the effects of a wind stress acting in the same direction of the density gradient, *i.e.*, same direction as the plume outflow. The observations were obtained during a period of wind blowing in the same direction as the along-shore pressure gradient. Experiment 4 also examined wind effects but in the opposite direction to the outflow. Experiments 5 and 6 examined the sensitivity of the results of the base case to the prescription of the longitudinal density gradient and to the depth of the water column, respectively. Experiments 7 and 8 investigated the sensitivity of the base case and of experiment 5 to the prescription of an initially homogeneous water column.

The one-dimensional (vertical) mixed layer numerical model solved the momentum equation and the salinity and temperature balances in the direction of the density gradient (along shore in this case). The values of the horizontal velocity component u (m s^{-1}), salinity S, temperature T (°C), and density ρ (kg m^{-3}) were estimated as a function of depth z (positive upwards) and time t at one vertical station with depth H equals 15 m, subdivided into 30 equally spaced levels. The dynamic balances were evaluated with time- and depth-varying turbulent (eddy) coefficients [A_v, A_{vS}, A_{vT} (m^2 s^{-1})] obtained from closure (Mellor and Durbin, 1975). The horizontal density gradient was prescribed as 3 kg m^{-3} in 10 km (or 4 salinity units), based on hydrographic observations collected in March 1996 and every month in the lower Chesapeake Bay (Valle-Levinson, unpublished data).

Governing Equations

The momentum balance included a barotropic and a baroclinic pressure gradient in the along-channel direction x and vertical mixing (vertical transfer of horizontal momentum):

$$\frac{\partial u}{\partial t} + g\frac{\partial \eta}{\partial x} + \frac{g}{\rho_0}\int_H^z \frac{\partial \rho}{\partial x} dz = \frac{\partial}{\partial z}[A_v \frac{\partial u}{\partial z}],$$

η was the surface elevation; g was the acceleration due to earth's gravity (9.8 m s^{-2}), ρ_0 was an average value of the density ρ; and A_v was the eddy diffusivity of momentum and was estimated according to the turbulence closure formulation of Mellor and Durbin (1975). This model, that also included an equation for the balance of dissolved oxygen, has been used by Valle-Levinson *et al.* (1995) to study hypoxia in western Long Island Sound.

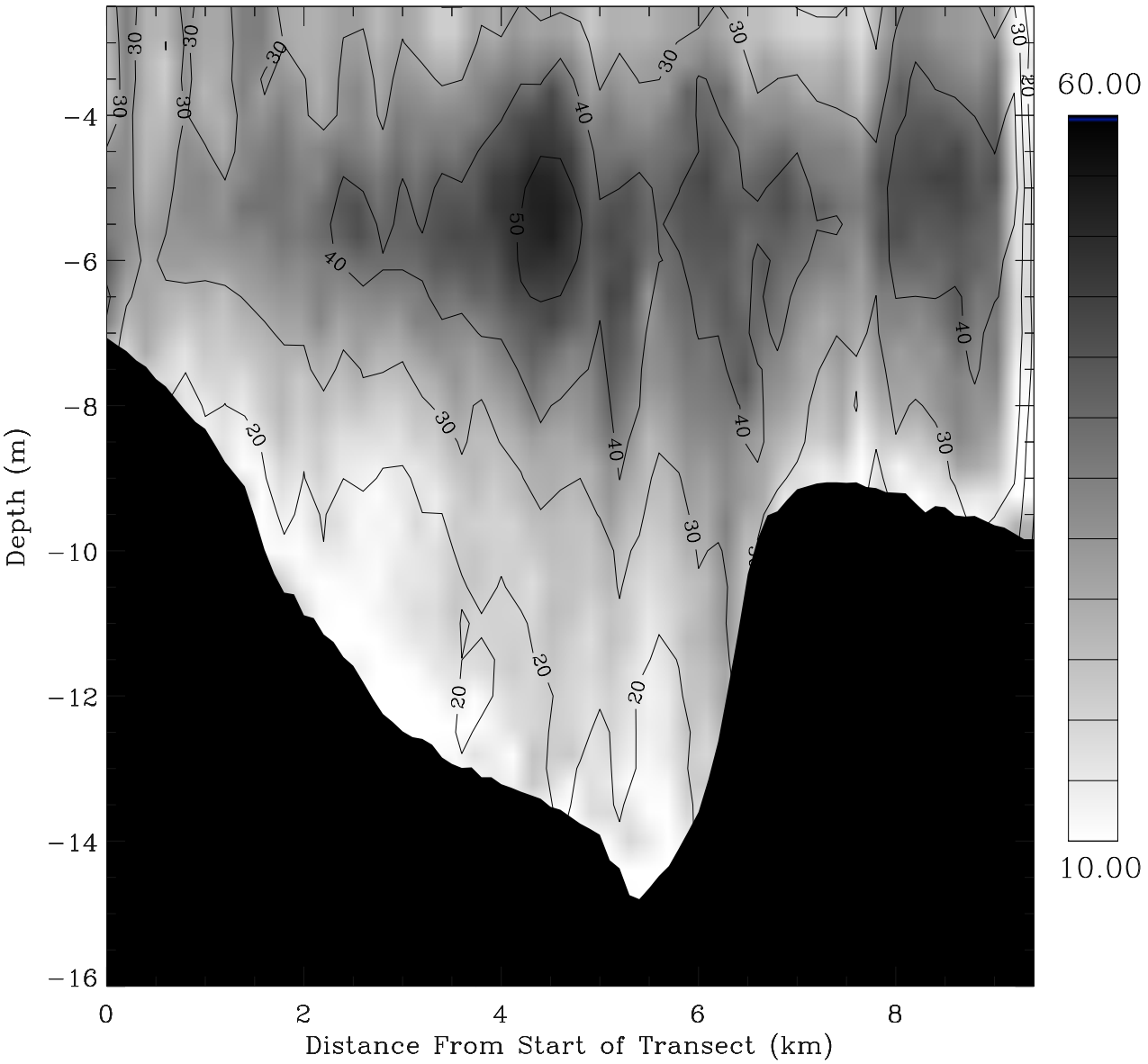
60.00
10.00
Depth (m)
−4
−6
−8
−10
−12
−14
−16
0
2
4
6
8
Distance From Start of Transect (km)

Experiment	Uo (m/s)	t_x (Pa)	DS/10 km	Depth (m)	DS (bot-top)
1	0.5	0	4	15	10
2	0.7	0	4	15	10
3	0.5	1	4	15	10
4	0.5	-1	4	15	10
5	0.5	0	1	15	10
6	0.5	0	4	12	10
7	0.5	0	4	15	0
8	0.5	0	1	15	0

Table 1. Summary of experiments carried out with the mixed layer model.

Intratidal variations of *T* and *S* were determined by a balance between vertical mixing and horizontal advection with horizontal gradients specified to be constant with depth and time:

$$\frac{\partial C}{\partial t} + u\frac{\partial C}{\partial x} = \frac{\partial}{\partial z}[A_{vC}\frac{\partial C}{\partial z}]$$

where *C* indicated the property of interest, *i.e.*, *T* or *S*, and A_{vC} represented the vertical eddy diffusivity coefficient. In this particular application, the vertical eddy diffusivity of heat, A_{vT}, was assumed equal to the vertical eddy diffusivity of salt, A_{vS}. Local density values were obtained from *T* and *S* using the equation of state of sea water (*e.g.* Gill, 1982, p. 599).

Boundary and Initial Conditions

For the momentum equation, quadratic surface and bottom shears were specified in the form: $A_v\, \partial u/\partial z = (\rho_a/\rho)\, C_D\, w\, |w|$, at the surface; and $A_v\, \partial u/\partial z = C_B\, w\, |w|$ at the bottom. The coefficient C_D represented nondimensional surface drag (0.0015); ρ_a was the air density (1.2 kg m^{-3}); *w* was the wind velocity, positive in the direction of the density gradient; and C_B was a nondimensional bottom drag coefficient (0.002). For temperature, a vertical heat flux *Q* could be specified at the surface, prescribed as zero here, and was negligible at the bottom. For salinity, it was assumed that there were no vertical fluxes of salt at either the air-water interface or the water-sediment interface. Experiments 1 through 6 began with vertically homogeneous *T* (17°C)

and a step in *S* between 5 and 6 m. The upper 5 m had homogeneous *S* of 20, and between 6 and 15 m the initial *S* was homogeneous at 30. Experiments 7 and 8 began with vertically homogeneous *S* of 30. As will be seen, the shape of the initial salinity profile played a minor role in determining the shape of the profile of the tidal current amplitude. A forcing velocity with *u* amplitude of 0.50 m s^{-1} (0.70 m s^{-1} for Experiment 2), oscillating at a frequency of $2\pi/12$ h was specified. Results represented the fifth tidal period after four tidal cycles of "spin-up" time as in Valle-Levinson and Wilson (1994).

Results of Simulations

The output of simulations was presented in Figure 7 that showed the time-depth variations of *u* and *S* within the tidal cycle, the amplitude of the tidal flow (determined with a least squares fit on the hourly flow values), and the corresponding tidal average of the vertical eddy viscosity. In the base case, the strongest ebb tidal currents (positive values) appeared at the surface as the barotropic pressure gradient from tidal forcing acted in concert with the baroclinic pressure gradient. This baroclinic pressure gradient was most positive at the surface because of its cumulative nature from bottom to surface. In contrast, the barotropic pressure gradient opposed the baroclinic pressure gradient during flood tidal currents and the strongest flood currents appeared under the surface, at the base of the pycnocline. This effect of the flood stages translated into tidal current amplitudes that increased with depth and reached a maximum at the pycnocline, as the measurements indicated (Fig. 6). The location of the core of maximum amplitude was related to the distribution of eddy viscosity (A_v) with depth, which was essentially zero between the surface and the base of the pycnocline. Vertical mixing was suppressed throughout that top 'slippery' layer and the energy of the flood currents was concentrated at approximately 5.5 m depth during most of the flood period. This base case could be considered as applicable to neap tides as was the case of the observations described before (Fig. 6).

The second experiment considered stronger tidal forcing than the base case to determine whether the core of maximum current amplitude changed depth. In this case, maximum ebb and maximum flood occurred at the surface (Fig. 7). Flood tidal currents were able to overcome the opposing baroclinic pressure gradient. As expected, stratification was weaker than in the base case and was even broken down by the end of flood. The coefficient A_v was non-zero everywhere in the water column and the tidal current amplitude was maximum at the surface and decreased with depth. The vertical migration of the core of maximum amplitude of semidiurnal tidal currents from the interior of the water column during neap tides to the surface during spring tides, has been observed in the James River (Valle-Levinson, Wong and Lwiza, in preparation). It is worth mentioning a cautionary note here because during spring tides, the semidiurnal tidal constituents (M_2, S_2, N_2) are in phase and the estimate of the semidiurnal (*e.g.* M_2) tidal current amplitude over one tidal cycle will reflect greater amplitudes than those during neap, when the constituents are in quadrature (90 degrees out of phase). Therefore, these results should be interpreted cautiously as they did not reflect time variations of one single tidal constituent but the interaction of several constituents of similar period, in this case, those near 12 hrs.

The next experiment (3) considered the effects of wind forcing in the same direction of the density gradient, *i.e.*, in the direction of ebb tidal currents and of the plume outflow. The

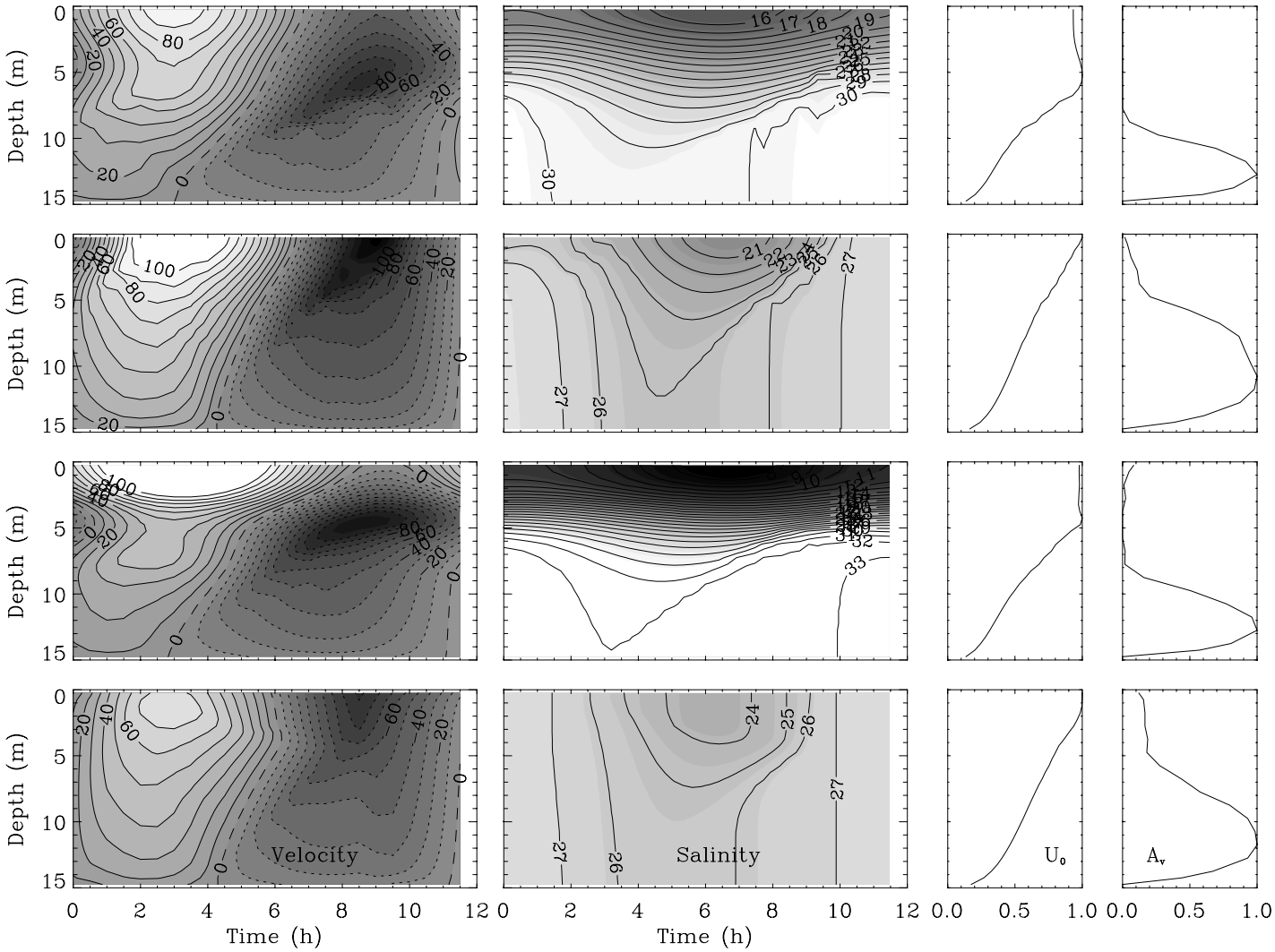

Figure 7. Results of experiments 1-4 of the one-dimensional mixed layer model. Panels in column one show variations of the tidal flow (centimeters per second) within the tidal cycle. Contour interval is 10 cm s^{-1}. Positive values (light areas) denote ebb flow. Panels in column two show variations in salinity within the tidal cycle. Contour interval is 1. Dark regions denote high salinity. Column three shows tidal amplitude (cm s^{-1}) scaled such that a value of 1.0 denotes maximum amplitude for the experiment. Column four shows tidal average of the vertical eddy viscosity (cm^2 s^{-1}) also scaled such that a value of 1.0 denotes maximum viscosity for the experiment. Values of maximum amplitude and viscosity for the four experiments are as follows: Exp 1: U0 78, Av 68; Exp 2: U0 118, Av 200; Exp 3: U0 82, Av 80; Exp 4: U0 76, Av 109.

behavior of the tidal currents and their amplitude was somewhat similar to that of the base case (Fig. 7). Obviously, ebb tidal currents were stronger in this experiment and flood tidal currents at the surface competed against the combined forcing from wind stress and baroclinic pressure gradient. Wind effects appeared only within the upper 8 m of the water column. In consequence, stratification was greatly enhanced as the wind mostly contributed to buoyancy advection because vertical mixing was restricted to a thin surface layer approximately 4 m thick, where the mean eddy viscosity was non-zero. The maximum amplitude of the tidal currents again appeared at the pycnocline region, where A_v was effectively suppressed. Under the wind-influenced layer, the profile of the mean eddy viscosity was essentially the same as the base case and reflected the exclusive effects of tidal forcing. This wind forcing enhanced the stratifying effects of tidal straining during ebb.

The effects of a wind blowing in the opposite direction to the density gradient (Experiment 4), *i.e.*, in the direction of flood tidal currents were analogous to the effects of strong tidal forcing (Fig. 7). In this case, ebb tidal currents were weaker than in the base case, which reduced the straining of the density field that favors stratification. After maximum ebb, the strongest ebb tidal currents appeared underneath the surface as wind forcing opposed the baroclinic pressure gradient and tidal forcing. On the other hand, the destratifying effects of tidal straining during flood were greatly enhanced by wind forcing. Stratification was much weaker than in previous cases and A_v was greater in general throughout the water column. This allowed the development of greatest tidal current amplitudes at the surface, where A_v was minimum, and decreasing with depth.

The effect of decreasing the longitudinal salinity gradient (Experiment 5) was to produce weak stratification (Fig. 8), non-zero eddy viscosities and tidal current amplitudes that decreased with depth. Decreased depth (Experiment 6) hindered the development of a sub-surface jet at the pycnocline because the baroclinic density gradient was not large enough (remember that this is an integration of the density gradient from bottom to surface, thus, the deeper the water column, the larger the baroclinic pressure gradient for a given longitudinal density gradient) to weaken barotropic flow (from flood tidal flows) at surface. Initial vertical homogeneity (Experiment 7) did not preclude the appearance of a subsurface maximum amplitude as stratification developed from the adjustment of the longitudinal density gradient. Initial vertical homogeneity and weak horizontal density gradient (Experiment 8) did preclude the appearance of a subsurface jet as mixing was non-zero throughout water column. Therefore, the conditions that combined to allow the development of a subsurface maximum in tidal current amplitude were weak tidal currents and winds blowing in the same direction as the surface density gradient, strong longitudinal density gradients, and moderate depths. All these conditions prevailed during the survey carried out in March of 1996 on the inner shelf to the south of the Chesapeake Bay mouth.

SUMMARY

The influence of buoyant discharges and bathymetry on semidiurnal tidal currents was investigated along an inner-shelf cross-shore transect outside of the Chesapeake Bay. Underway measurements of current velocity obtained with an ADCP and of near-surface temperature and salinity were carried out during one semidiurnal tidal cycle (12 hours) on March 26-27, 1996. These observations reflected the forcing of winds from the NNE and high discharge conditions.

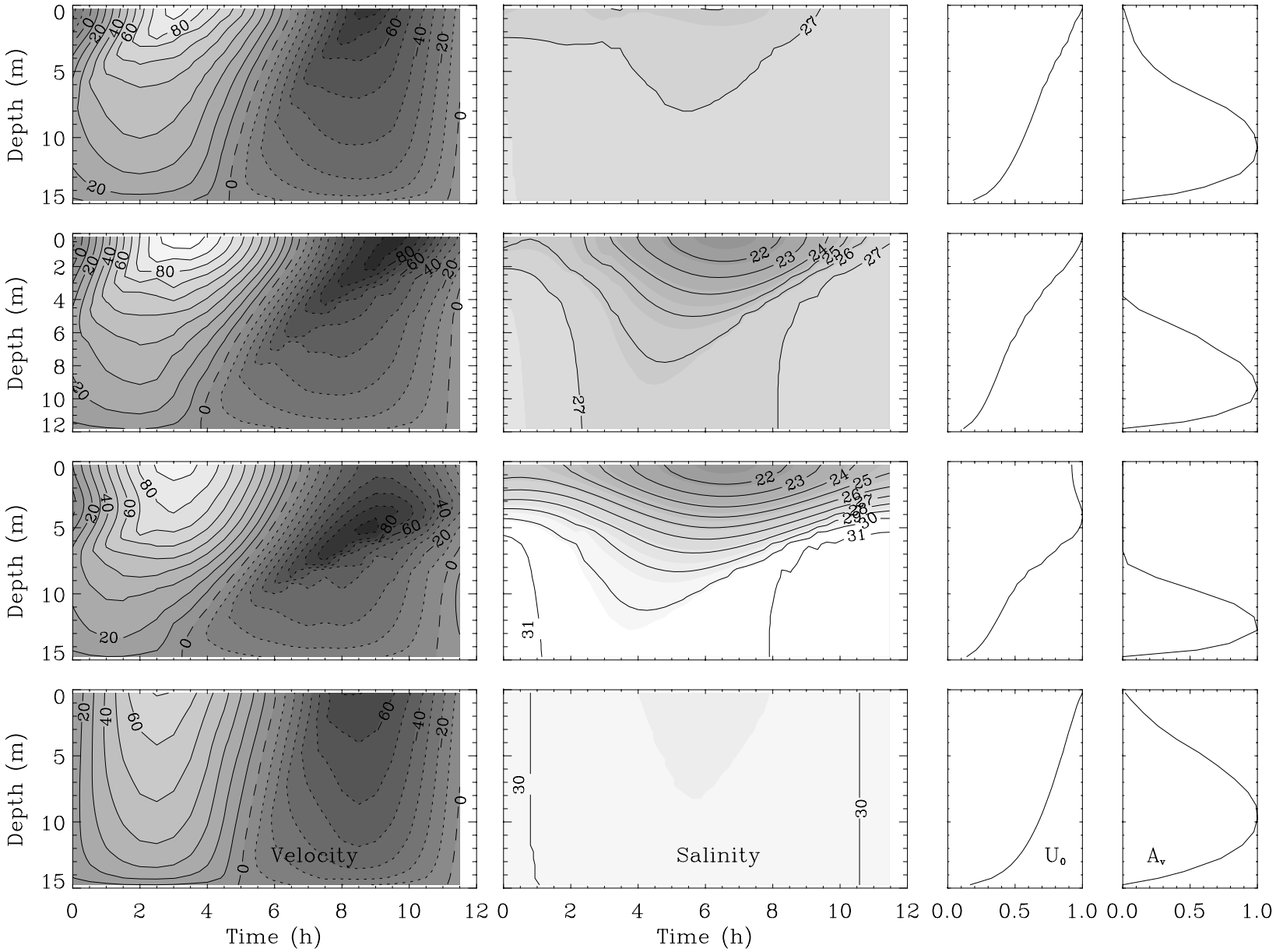

Figure 8. Results of experiments 5-8 of the one-dimensional mixed layer model. Description follows that of Figure 7. Values of maximum amplitude and viscosity for the four experiments are as follows: Exp 5: U0 78, Av 140; Exp 6: U0 96, Av 97; Exp 7: U0 81, Av 83; Exp 8: U0 69, Av 102.

The year of 1996 began with the wettest January and became the wettest year on record according to the USGS. The subtidal and semidiurnal tidal contributions to the data collected were separated using a least squares technique.

The subtidal flow along the shelf showed values that reached 0.55 m s^{-1} within the southward flowing plume of the Chesapeake Bay. The outflow developed over an ambient subtidal current that also flowed to the south throughout the section measured. The cross-shore component of the subtidal flow was in general directed onshore thus suggesting that the transect was located within the quasi-geostrophic turning region of the Chesapeake Bay plume. The surface salinity and temperature values displayed an along-shore front that delimited the offshore extent of the plume. The location of the plume front over the channel coincided with the offshore limit of the core of subtidal flow attributed to the plume.

The buoyant discharge related to the plume and the channel-shoals bathymetry noticeably modified the phase and amplitude of the semidiurnal tidal currents. The phase of the tidal currents inside the plume lagged behind the currents over the adjacent waters by approximately 80 minutes. Also, the phase inside the channel lagged behind the surrounding water due to the combined effects of bottom friction (less in the channel) and inertia (more in the channel). The amplitude of the tidal currents exhibited a maximum centered over the channel due to reduced friction there. The maximum amplitude was located at a depth of approximately 5 m in response to the decreased turbulent vertical eddy viscosity near the pycnocline, as shown by a one-dimensional mixed layer model.

A total of eight experiments with the mixed-layer model were carried out to investigate the effects of tidal forcing, wind stress, water column depth, and vertical and horizontal density gradients on the profile of the tidal current amplitude and the development of a subsurface maximum. This subsurface maximum formed under the combined influence of strong horizontal salinity gradients (4 units in 10 km), relatively weak tidal (0.5 m s^{-1}) and wind (< 0.1 Pa) forcing, and relatively deep (> 15 m) regions. It appeared in the zone of the pycnocline where turbulence was suppressed, as indicated by zero vertical eddy viscosities, thus eliminating any vertical transfer of horizontal momentum. The initial salinity (or density) profile prescribed in the model did not have a significant influence in altering the profile of the tidal current amplitude. The subsurface maximum in tidal current amplitude migrated to the surface with weaker salinity gradients, stronger tidal currents, stronger wind velocities (or winds blowing in the direction opposite to the baroclinic flow at the surface), or shallower water column depths than those mentioned above.

The results of this study suggested that the tidal currents on an inner shelf can be affected by both the plume of buoyant water flowing from an estuary and by any possible abrupt bathymetric changes of the area.

REFERENCES

Boicourt W. C. (1973) The circulation of water on the continental shelf from Chesapeake Bay to Cape Hatteras, Ph.D. Thesis, John Hopkins University, Baltimore, MD, 183 pp.

Boicourt W. C. (1981) Circulation in the Chesapeake Bay entrance region: estuary-shelf interaction. In: *Chesapeake Bay Plume Study: Superflux 1980*, NASA Conference Publication 2188, J. Campbell and J. Thomas, editor, Hampton, VA, pp. 61-78.

Browne D. R. and C. W. Fisher (1988) Tide and tidal currents in the Chesapeake Bay. NOAA Technical Report NOS OMA 3, U.S. Department of Commerce, Washington, DC, 84 pp.

Chao S.-Y. (1988) River-forced estuarine plumes. *Journal of Physical Oceanography*, **18**, 72-88.

Chao S.-Y. and W. C. Boicourt (1986) Onset of estuarine plumes. *Journal of Physical Oceanography*, **16**, 2137-2149.

Fisher C. W. (1986) Tidal circulation in Chesapeake Bay. Ph.D. Dissertation, Old Dominion University, Norfolk, VA, 255 pp.

Gill, A. E. (1982) *Atmosphere-Ocean Dynamics*, Academic Press, San Diego, CA. 662 pp.

Huzzey L. M. (1982) The dynamics of a bathymetrically arrested estuarine front. *Estuarine, Coastal & Shelf Science*, **15**, 527-552.

Johnson, D. R. (1985) Wind-forced dispersion of blue crab larvae in the Middle Atlantic Bight. *Continental Shelf Research*, **4**, 733-745.

Joyce T. M. (1989) On in situ "Calibration" of Shipboard ADCPs. *J. Atmos. Oceanic Technol.*, **6**, 169-172.

Kapolnai A., F. E. Werner and J. O. Blanton (1996) Circulation, mixing and exchange processes in the vicinity of tidal inlets: A numerical study. *Journal of Geophysical Research*, **101**, 14,253-14,268.

Largier J. L. and S. Taljaard (1991) The dynamics of tidal intrusion retention and removal of seawater in a bar-built estuary. *Estuarine, Coastal & Shelf Science*, **33,** 325-338.

Largier J. L. (1992) Tidal intrusion fronts. *Estuaries*, **15,** 26- 39.

Lwiza K. M. M., D. G. Bowers and J. H. Simpson (1991) Residual and tidal flow at a tidal mixing front in the North Sea. *Continental Shelf Research*, **11**, 1379-1395.

Mellor G. L. and P. A. Durbin (1975) The structure and dynamics of the ocean surface mixed layer. *Journal of Physical Oceanography*, **5**, 718-728.

Münchow A., A. K. Masse and R. W. Garvine (1992) Astronomical and nonlinear tidal currents in a coupled estuary shelf system. *Continental Shelf Research*, **12**, 471-498.

Noble, M. A., W. W. Schroeder, W. J. Wiseman Jr., H. F. Ryan, and G. Gelfenbaum (1996) Subtidal circulation patterns in a shallow, highly stratified estuary: Mobile Bay, Alabama. J. Geophys. Res. **101(C11)**. 25,689-25,703.

Paraso M. C. and A. Valle-Levinson (1996). Atmospheric forcing effects on sea level and water temperature in the lower Chesapeake Bay: 1992. *Estuaries*, **19(3)**, 548-561.

Redfield A. C. (1958) The influence of the continental shelf on the tides of the Atlantic coast of the United States. *Journal of Marine Research*, **16**, 432-448.

Sanders T. M. and R. W. Garvine (1996) Frontal observations of the Delaware Coastal Current source region. *Continental Shelf Research*, **16**, 1009-1021.

Simpson J. H. and A. J. Souza (1995) Semidiurnal switching of stratification in the region of freshwater influence of the Rhine. *Journal of Geophysical Research*, **100**, 7037-7044.

Souza A. J. and J. H. Simpson (1996) The modification of tidal ellipses by stratification in the Rhine ROFI. *Continental Shelf Research*, **16**, 997-1007.

Turner, J.S. (1973) *Buoyancy effects in fluids*. 367 pp. Cambridge University Press, New York.

Valle-Levinson A. (1995) Observations of barotropic and baroclinic exchanges in the lower Chesapeake Bay. *Continental Shelf Research*, **15**, 1631-1647.

Valle-Levinson A. and K. M. M. Lwiza (1997) Bathymetric influences on the lower Chesapeake Bay Hydrography. *Journal of Marine Systems*, in press.

Valle-Levinson A., J. M. Klinck and G. H. Wheless (1996) Inflows/outflows at the transition between a coastal plain estuary and the coastal ocean. *Continental Shelf Research*, **16**, 1819-1847.

Valle-Levinson A. and K. M. M. Lwiza (1995) The effects of channels and shoals on exchange between the Chesapeake Bay and the adjacent ocean. *Journal of Geophysical Research*, **100,** 18551-18563.

Valle-Levinson, A. and R. E. Wilson (1994) Effects of sill bathymetry, oscillating barotropic forcing, and vertical mixing on estuary/ocean exchange. *Journal of Geophysical Research*, **99,** 5149-5169.

Weaver A. T. and W. W. Hsieh (1987) The influence of buoyancy flux from estuaries on continental shelf circulation. *Journal of Physical Oceanography*, **17**, 2127-2140.

Wheless G. H. and A. Valle-Levinson (1996) A modeling study of tidally driven estuarine exchange through a narrow inlet onto a sloping shelf. *Journal of Geophysical Research*, **101(C11)**, 25,675-25,687.